

Intermediate phase, network demixing, boson and floppy modes, and compositional trends in glass transition temperatures of binary $\text{As}_x\text{S}_{1-x}$ system

Ping Chen, Chad Holbrook, and P. Boolchand

Department of Electrical and Computer Engineering, University of Cincinnati, Cincinnati, Ohio 45221-0030, USA

D. G. Georgiev

Department of Electrical Engineering and Computer Science, University of Toledo, Toledo, Ohio 43606, USA

K. A. Jackson

Department of Physics, Central Michigan University, Mount Pleasant, Michigan 48859, USA

M. Micoulaut

Laboratoire de Physique Theorique de la Matiere Condensée, University Pierre et Marie Curie, Boite 121, 4 Place Jussieu, 75252 Paris Cedex 05, France

(Received 12 October 2008; revised manuscript received 13 November 2008; published 30 December 2008)

The structure of binary $\text{As}_x\text{S}_{1-x}$ glasses is elucidated using modulated differential scanning calorimetry, Raman scattering, IR reflectance, and molar volume experiments over a wide range ($8\% < x < 41\%$) of compositions. We observe a reversibility window in the calorimetric experiments, which permits fixing the three elastic phases: *flexible* at $x < 22.5\%$, *intermediate* in the $22.5\% < x < 29.5\%$ range, and *stressed rigid* at $x > 29.5\%$. Raman scattering supported by first-principles cluster calculations reveals that the observed vibrational density of states has features of both pyramidal (PYR) $[\text{As}(\text{S}_{1/2})_3]$ and quasitetrahedral (QT) $[\text{S} = \text{As}(\text{S}_{1/2})_3]$ local structures. The QT unit concentrations show a global maximum in the intermediate phase (IP), while the concentration of PYR units becomes comparable to those of QT units in that phase, suggesting that both these local structures contribute to the width of the IP. The IP centroid in the sulfides is shifted to lower As content x than in corresponding selenides, a feature identified with excess chalcogen partially segregating from the backbone in the sulfides, but forming part of the backbone in selenides. These ideas are corroborated by the proportionately larger free volumes of sulfides than selenides and the absence of chemical bond-strength scaling of T_g 's between As sulfides and As selenides. Low-frequency Raman modes increase in scattering strength almost linearly as As content x of glasses decreases from $x=20\%$ to 8% and glasses become flexible, with a slope that is close to the floppy mode fraction predicted by rigidity theory. These results show that floppy modes contribute to the excess vibrations observed at low frequency. In the intermediate and stressed rigid elastic phases low-frequency Raman modes persist and are identified as boson modes. Some consequences of the present findings on the optoelectronic properties of these glasses are commented upon.

DOI: [10.1103/PhysRevB.78.224208](https://doi.org/10.1103/PhysRevB.78.224208)

PACS number(s): 63.50.Lm, 78.30.Ly, 65.60.+a

I. INTRODUCTION

Network glasses have traditionally been modeled as continuous random networks (CRNs). The description has worked well for several stoichiometric oxides but less so for chalcogenides. Some chalcogenides macroscopically phase separate displaying bimodal T_g 's, as in the case of the Ag–Ge–Se ternary,^{1,2} materials that serve as active media in programmable nonvolatile memories used for portable electronics.³ In bulk glasses of the Ag–Ge–Se ternary, the nature of the two glass phases has also been established by calorimetry^{4,5} and electric force microscopy.⁶ Furthermore, even in chalcogenides that display a single T_g , demixing of networks can occur on nanoscale as either monomers or even large clusters decouple from the backbone and enrich their functionality in remarkable ways. It is in this respect that the case of the binary $\text{As}_x\text{S}_{1-x}$ glass system has received attention^{7–12} over the years starting from the early work of Ward¹³ at Xerox, who recognized S_8 rings to decouple in S-rich glasses. It is generally believed that As serves the role of cross-linking chains of sulfur to acquire a local threefold

coordination as in a pyramidal (PYR) unit $\text{As}(\text{S}_{1/2})_3$, and at the stoichiometric composition $x=40\%$, a CRN of S-bridging pyramidal units is realized.¹⁴ Close analogies in molecular structure of the stoichiometric glass with the layered structure of $c\text{-As}_2\text{S}_3$ (orpiment) have been drawn. The molecular structure of As_2S_3 glass has also been compared to that of As_2Se_3 glass. If these stoichiometric glasses were to form CRNs, then their mean coordination number, $r=2.40$, and following the ideas of Phillips¹⁵ and Thorpe,¹⁶ the count of Lagrangian bonding constraints per atom, $n_c=3$, for both these glasses.¹⁷ Their glass structures can then be expected to be optimally constrained and to possibly self-organize¹⁸ to produce rigid but unstressed structures. Such a picture appears to largely describe the structure of As_2Se_3 glass,¹⁹ a composition that is almost in the reversibility window of binary $\text{As}_x\text{Se}_{1-x}$ glasses.¹⁹ On the other hand, the stoichiometric composition, As_2S_3 , is far from being in the reversibility window of binary $\text{As}_x\text{S}_{1-x}$ glasses, as will be shown in the present work. The underlying differences of structure between As-sulfide and -selenide glasses are not confined to the stoichiometric composition; in fact they extend to all other

compositions as well. Do these peculiarities of structure of As–S glasses occur in other group-V and group-IV sulfides? We comment on the issue as well.

Glass transition temperatures (T_g 's) provide a good measure²⁰ of network connectivity. For glass networks possessing the “same” connectivity, T_g 's usually scale with strengths of chemical bonds. For example, in comparing binary $[\text{Ge}_x\text{X}_{1-x}]$ ($X=\text{S}$ or Se) and ternary $[\text{P}_x\text{Ge}_x\text{X}_{1-2x}]$ ($X=\text{S}$ or Se) glasses, one generally finds the ratio of T_g 's of sulfides to selenides to scale as the ratio of single chemical bond strengths.²¹ However, such is not the case for the $\text{As}_x\text{X}_{1-x}$ binaries ($X=\text{S}$ or Se). For example, T_g of As_2S_3 [205(2) °C] (Ref. 22) is almost the same as that of As_2Se_3 [197(2) °C].^{8,19} If these glasses were to possess the same network connectivity, one would have expected T_g of As_2S_3 to be 13% higher (255 °C) than of As_2Se_3 since single As–S covalent bonds²³ (47.25 kcal/mole) are 13% stronger than single As–Se covalent bonds (41.73 kcal/mole). The absence of bond-strength scaling of T_g is not restricted to the stoichiometric composition, $x=40\%$, but it occurs at other As concentrations x as well. These data suggest that there are intrinsic differences of glass structure between As sulfides and selenides.

Differences of glass structure between As sulfides and As selenides have a bearing on infrared optical^{24,25} applications of these materials. Photodarkening in amorphous films of As_2S_3 and As_2Se_3 has been examined²⁶ using near band-gap light (500 nm for $a\text{-As}_2\text{S}_3$ film and 650 nm for $a\text{-As}_2\text{Se}_3$ film). The results show that not only band-gap reduction but also rate of photodarkening is higher in the sulfide than in the selenide films. These glasses also display large optical nonlinearities, low phonon energies, and low nonlinear absorption.²⁷ Material properties such as nonlinear changes in refractive index, electronic polarizability, molecular orientation, electrostriction, and thermal effects are of relevance in this context.²⁸ Among these, fast electronic nonlinearity is of particular interest; it is determined by electron distribution in various local structures and can be expected to change with glass composition. Thus, introduction of Se in As–S glasses increases the nonresonant refractive nonlinearity up to 400 that of fused silica.²⁹ In ternary Ge–As–Se glasses, it has been shown that substitution of Ge by As promotes while replacement of Se by As suppresses optical nonlinearity.³⁰ Furthermore, refractive nonlinearity is found to vary with composition in overconnected ($r>2.4$) glasses with the nonlinearity being highest for the lowest Ge concentration.³¹ The microscopic origin of these nonlinear effects remains an open question in the field. It is likely that a basic understanding of glass structure would help in addressing the underlying issues.

In the present work we focus on compositional dependence of glass structure; we have examined the thermal [modulated differential scanning calorimetry (DSC) (m-DSC)] and optical (Raman and IR reflectance) behavior of bulk $\text{As}_x\text{S}_{1-x}$ glasses over a wide range of compositions, $8\%<x<41\%$. In Raman-scattering compositional trends in vibrational modes at low-frequency (0–100 cm^{-1}), bond-bending (100–250 cm^{-1}), and bond-stretching (250–500 cm^{-1}) regimes are analyzed. Results of first-principles cluster calculations³² are used to analyze the Ra-

man and IR vibrational density of states. The present data suggest that in addition to threefold coordinated As, quasi-fourfold coordinated As local structures (with As having three bridging and one nonbridging S neighbors) are also present in the S-rich glasses. Both these local structures are found in binary P–S (Refs. 21, 33, and 34) and P–Se glasses.^{35,36} Our m-DSC experiments reveal the existence of a reversibility window³⁷ in the $22\%<x<29\%$ range, an observation that fixes the three elastic phases, flexible, intermediate, and stressed rigid, in the present As–S binary. The window is found to be shifted to lower As content x in relation to the one in corresponding selenides. We trace the observation to partial demixing of excess S from networks of the present sulfides in sharp contrast to the complete mixing of excess Se in the corresponding selenides. The strongly excited low-frequency Raman modes, also called boson modes, are analyzed in the present sulfide glasses. In the elastically flexible regime ($x<20\%$) these low-frequency vibrations are shown to come from *floppy modes*, while those in the intermediate and elastically stressed-rigid glasses probably come from intercluster soft modes.

In Sec. II we present some background considerations to understand compositional trends in T_g . Results of first-principles cluster calculations to analyze the Raman vibrational modes are presented in Sec. III. Experimental results and their discussion in relation to issues of glass molecular structure, floppy modes, boson modes, and the three elastic phases in the present As–S binary appear in Secs. IV and V, respectively. A summary of the present findings appears in Sec. VI.

II. COMPOSITIONAL TRENDS IN T_g AND GLASS STRUCTURE

A. Stochastic agglomeration and network connectivity

A useful means to understand T_g variation with glass chemical composition or network structure is provided by a stochastic agglomeration theory (SAT). The theory allows a prediction of T_g with modifier composition when agglomeration of atoms forming part of a glass-forming liquid proceeds in a *stochastic fashion*. The central idea of the theory^{20,38,39} is to relate an increase in viscosity to network formation as chemical bonds between well-defined *local structures* are formed at random upon cooling. For a base glass composed of A atoms, which is modified by alloying B atoms, i.e., an A_xB_{1-x} binary system, theory predicts^{20,38,39} a parameter-free slope of T_g with glass composition x in the limit when x is low,

$$\left[\frac{dT_g}{dx} \right]_{x=0, T_g=T_{g0}} = \frac{T_{g0}}{\ln \left[\frac{r_B}{r_A} \right]}. \quad (1)$$

In Eq. (1), r_B and r_A are the coordination numbers of the additive atom B and the atom A comprising the base glass network and T_{g0} represents the glass transition temperature of the base material. The denominator appearing in Eq. (1) gives an entropic measure of network connectivity,⁴⁰ and the

lower the entropy the higher the slope of T_g with x . For the case of SiO_2 , which has a large $T_{g0} \sim 1200^\circ\text{C}$, a large slope dT_g/dx is expected and indeed found in sodium silicate glasses in the low modified regime. For the case of $\text{As}_x\text{Se}_{1-x}$ ($r_A=2$), and if we take As atoms to be threefold coordinated ($r_B=3$), one expects the slope to be $6.17^\circ\text{C/mol}\%$ of As. The observed slope is found³⁶ to be $4.1^\circ\text{C/mol}\%$ of As. We have suggested in earlier work⁵ that the presence of fourfold coordinated As as in a quasitrahedral (QT) unit will increase the number of ways to connect arsenic and selenium atoms together and will thus decrease the slope dT_g/dx and permit one to reconcile the observed slope dT_g/dx if the concentration of such units is in the (20–30)% range.

Elemental Se is a good glass former composed largely of polymeric chains of selenium. On the other hand, elemental S melts upon cooling condense into a molecular solid composed of S_8 rings. These considerations help us reconcile why binary $(\text{Ge or As})_x\text{Se}_{1-x}$ melts give rise to homogeneous glasses extending all the way to pure Se, while corresponding sulfide melts, in general, segregate into a glassy backbone and S_8 crowns as x decreases to ~ 0.20 ; and as x approaches 0, melts spontaneously crystallize. The present $\text{As}_x\text{S}_{1-x}$ binary glasses intrinsically segregate on a molecular scale as x approaches 0, so that SAT as we know cannot be directly applied. Inferring aspects of glass structure at low x using SAT poses new challenges. Fortunately, signature of S_8 rings segregating from the backbone in sulfide glasses comes independently from Raman scattering and modulated DSC experiments as will be illustrated in the present work. Many of these ideas were known more than 25 years ago. What is different, however, is that the use of m-DSC has now permitted establishing scan-rate-independent glass transition temperatures (T_g 's). At higher x when network formation is well developed, trends in T_g can be understood in terms of SAT. These thermal data complemented by optical ones (Raman and IR reflectance measurements) afford other insights into the molecular structure of the present sulfide glasses as we shall illustrate in this work.

B. Chemical bond-strength rescaling of glass transition temperatures

The importance of network connectivity in determining the T_g of network glasses has evolved elegantly from SAT. The importance of chemical bond strengths in determining T_g was emphasized by Tichý and Tichá⁴¹ from empirical considerations. It is becoming transparent that bond-strength scaling of T_g 's does occur but only if the underlying network structures being compared possess the same connectivity. An illustrative example is the case of the $\text{Ge}_x\text{P}_x\text{X}_{1-2x}$ ternaries with $X=\text{Se}$ or S (Fig. 1). A perusal of the data^{42,43} shows that in the $10\% < x < 18\%$ range, T_g ratio of sulfide to selenide glasses is found to be 1.13, and the ratio is found to be independent of x . The finding illustrates that connectivity of underlying backbones steadily increases as the concentration x of the cross-linking atoms P and Ge increases in both these systems. We understand the scaling factor of 1.13 in terms of the higher chemical bond strength of Ge–S and P–S bonds in relation to Ge–Se and P–Se ones. The Pauling single bond-

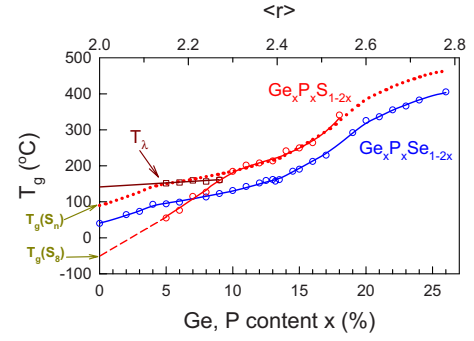


FIG. 1. (Color online) Glass transition temperature in $\text{Ge}_x\text{P}_x\text{S}_{1-2x}$ (Ref. 42) and $\text{Ge}_x\text{P}_x\text{Se}_{1-2x}$ (Ref. 43) ternaries compared. In the $10\% < x < 18\%$ range one observes scaling of T_g with chemical bond strengths. At low x ($< 10\%$), S_8 rings steadily demix, sulfur polymerization transition T_λ is manifested, and T_g 's steadily decline in the sulfide glasses.

strength data²³ on the underlying bonds are as follows: Ge–S bond, $E_b=55.52$ kcal/mol; Ge–Se bond, $E_b=49.08$ kcal/mol; P–S bond, $E_b=54.78$ kcal/mol; and P–Se bond, $E_b=49.72$ kcal/mol. These data yield the ratio of chemical bond strengths of the P and Ge sulfide bonds to corresponding selenide bonds of 1.12. These ideas on bond-strength rescaling of T_g 's will be useful when we visit results on the present As–S glasses and compare them to those on corresponding selenides.

At $x < 10\%$, a rescaling of T_g 's no longer holds since in the sulfide glasses S_8 rings steadily decouple leading to loss of a network, while in the selenides a network structure continues to persist even as x approaches 0. The signature of S_8 ring decoupling is the appearance of the T_λ transition (Fig. 1). T_g 's in the $10\% > x > 0\%$ range decrease almost linearly to extrapolate to a value of about -50°C as x approaches 0. We assign the extrapolated $T_g=-50^\circ\text{C}$ to that of a S-ring glass. On the other hand, if one linearly extrapolates the $T_g(x)$ data from $x \sim 10\%$ backward to $x=0$, one obtains an extrapolated T_g of about 100°C . We assign the extrapolated T_g of 100°C to that of a S_n -chain glass. These extrapolated T_g values of a S-chain and a S-ring glass are independently corroborated by results on several other binary and ternary sulfide glass systems.

III. FIRST-PRINCIPLES CLUSTER CALCULATIONS OF VIBRATIONAL DENSITY OF STATES

To investigate the origin of key features in the Raman spectra of $\text{As}_x\text{S}_{1-x}$ glasses, we conducted first-principles calculations based on density-functional theory in the local-density approximation (LDA).⁴⁴ The calculations were performed using the NRLMOL code.^{45,46} Extensive Gaussian basis sets were used to represent the electronic orbitals. Pseudopotentials⁴⁷ were used for the As and S atoms, while H atoms were treated³² in an all-electron format.

Attention was focused on two structural building blocks of the glasses, the As-S_3 PYR and the QT As-S_4 units, both shown in Fig. 2. Hydrogen atoms were added to the three basal S atoms in each of these models to tie off dangling

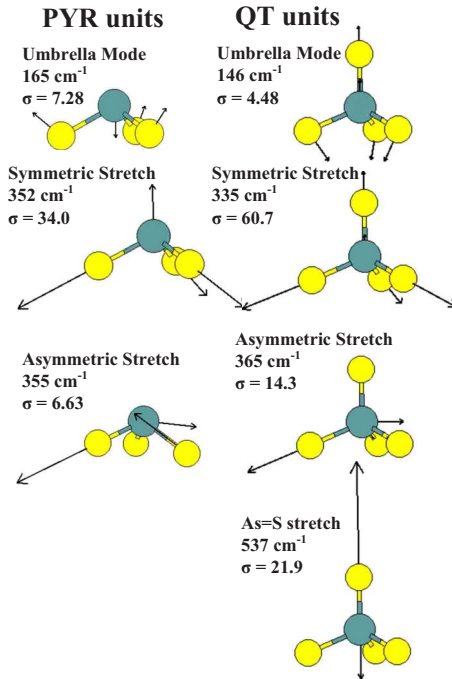


FIG. 2. (Color online) Eigenvectors and eigenfrequencies of pyramidal (left column) and quasitetrahedral (right column) local structures obtained from first-principles cluster calculations. Dark (blue-green) and light (yellow) atoms represent arsenic and sulfur, respectively. Mode frequencies and Raman cross sections (σ) are indicated with each vibrational mode. See Table I for a summary of results.

bonds so as to better mimic the local chemistry of these units in the glass. The S–H bonds nominally represent S–As bonds to the glass network. The Pauling electronegativities of As and H are 2.18 and 2.20, respectively, so that one expects S–H and S–As bonds to have very similar polarities. The cluster bond lengths and bond angles were relaxed to a minimum-energy configuration and the vibrational normal modes of the clusters were calculated using a standard technique.⁴⁸ IR intensities and Raman activities for the vibrational modes were then calculated within the LDA. The method has been described fully elsewhere.⁴⁸ Briefly, IR intensities and Raman activities can be related to changes in

cluster dipole moments and polarizabilities caused by atomic displacements in the vibrational modes. These changes can be computed directly within the LDA, using no adjustable parameters or empirical input. Calculated results for a diverse set of molecules have been shown to be in good agreement with experimental measurements.⁴⁸

The results for the PYR and QT units are given in Table I. Mode frequencies and total IR intensities and Raman activities for key vibrational modes are listed. Normal mode eigenvectors indicating the pattern of atomic displacements in each mode are shown in Fig. 2. It is interesting to note that the symmetric and asymmetric modes associated with the PYR unit are nearly degenerate at 352 and 355 cm^{-1} , respectively, while the analogous modes in the QT unit are split at 335 and 365 cm^{-1} . (The asymmetric stretch modes in both models are doubly degenerate.) Only one set of eigenvectors is shown for each model in Fig. 2. The QT unit also features a mode at 537 cm^{-1} that arises from a stretch of the bond between As and the onefold coordinated S atom. This mode clearly has no analog in the PYR model and is well separated from the remaining As–S stretch modes. The results, presented in Table I and Fig. 2, are discussed further below.

IV. EXPERIMENTAL

A. Sample synthesis

Figure 3 shows the phase diagram of the As–S binary system.^{49,50} In the phase diagram, the crystalline phases shown are crystalline S_8 that exist in three forms⁵¹ (α , β , and γ), $c\text{-As}_2S_3$ (orpiment),⁵² $c\text{-As}_4S_4$ (realgar) that exists in two forms⁵³ (α , β), and $c\text{-As}_4S_3$ (dimorphite) that exists in three forms⁵⁰ (α , β and γ). Both crystalline As_4S_4 and As_4S_3 are molecular crystals composed of monomers. A perusal of the As_xS_{1-x} phase diagram shows that there is a eutectic near $x \sim 1\%$. The glass-forming range in the As_xS_{1-x} binary extends from about $5\% < x < 55\%$ range. At $x < 5\%$ melts are largely composed of S_8 rings, while at $x > 55\%$ melts crystallize into realgar or As_4S_3 monomers. Other crystalline forms found in mineral data include As_4S (duranusite)⁵⁴ and As_4S_5 (uzonite).⁵⁵

Glass samples of typically 2 g in size were synthesized using 99.999% As_2S_3 and elemental S pieces from Cerac Inc.

TABLE I. Raman and IR vibrational modes of As–S clusters. The frequencies and Raman/IR cross sections and depolarization ratios for each cluster are given, along with a description of the eigenvectors.

Cluster	ω (cm^{-1})	IR	I^{Ram}			ρ	Description
			Iso.	Total			
AsS_3H_3	165	0.18	5.0	7.28	0.23	Umbrella	
	352	0.18	31.3	34.0	0.06	Symmetric stretch	
	355	0.78	0.00	6.63	0.75	Asymmetric stretch	
AsS_4H_3	146	0.20	1.10	4.48	0.57	Umbrella	
	335	0.21	59.5	60.7	0.01	Symmetric stretch	
	365	1.17	0.00	14.3	0.75	Asymmetric stretch	
	537	1.58	12.1	21.9	0.34	S=As	

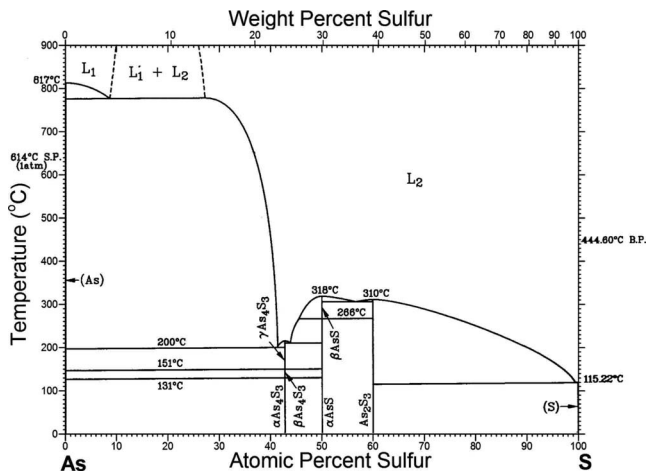


FIG. 3. Phase diagram of $\text{As}_x\text{S}_{1-x}$ binary taken from the work of Blachnik *et al.* (Ref. 49) and Ref. 50. There is a eutectic near $x \sim 1\%$ but none in the region $40\% < x < 1\%$ of As where the reversibility window is observed in the present work.

The starting materials were weighed and mixed in a N_2 gas purged glove bag and then sealed in evacuated ($<10^{-7}$ Torr) dry quartz tubings of 5.0 mm internal diameter and 1 mm wall thickness. Temperature of quartz tubes was slowly increased to 650 °C at a rate of 1 °C/min. Melts were homogenized by mixing them at 600 °C for 2 days or longer (see below). Glass samples were realized by quenching melts from 50 °C above the liquidus⁴⁹ into cold water. Once quenched, glass sample homogeneity was ascertained by FT-Raman scattering along the length of sealed quartz tubes used to synthesize samples. Periodic evaluation of samples with increasing reaction time of melts at 650 °C revealed that Raman line shapes became indistinguishable only after melts were homogenized for typically 2–3 days. Once samples were synthesized, these were stored in evacuated Pyrex ampoules to avoid hydrolysis.

B. Molar volumes

An 8-in.-long quartz fiber suspended from a pan of digital balance (Mettler model B154) and a hook to support a sample at the far end was used to measure mass densities using the Archimedes principle. Glass samples of typically 100 mg or larger in size were weighed in air and in pure ethyl alcohol. The density of alcohol was calibrated using a single-crystal bulk piece of Si and Ge as density standards. With the arrangement, we could obtain the mass density of samples to an accuracy of 3/4 % or less. Resulting molar volumes as a function of glass composition are summarized in Fig. 4 and show that $V_m(x)$ decreases with increasing x but with a local minimum in the $20\% < x < 28\%$ range, the reversibility window (see below). For comparison we have also included in Fig. 4, molar volumes on corresponding $\text{As}_x\text{Se}_{1-x}$ glasses taken from the work of Georgiev *et al.*¹⁹ We shall return to discuss these results later.

C. Modulated differential scanning calorimetry

Glass transition properties were examined using a modulated DSC, model 2920 from T.A. Instruments. Typically

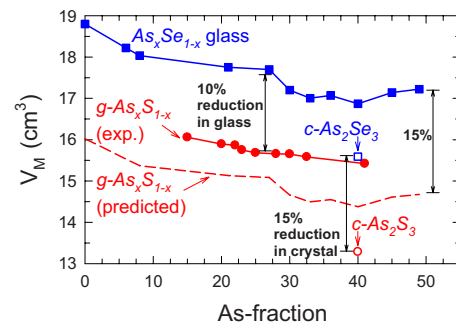


FIG. 4. (Color online) Variations in molar volumes of $\text{As}_x\text{S}_{1-x}$ (● red, present work) and $\text{As}_x\text{Se}_{1-x}$ glasses (■ blue) taken from the work of Georgiev *et al.* (Ref. 19). Molar volumes of crystalline As_2S_3 (○, Ref. 83) is found to be 15% lower than that of $c\text{-As}_2\text{Se}_3$ (□, Ref. 84). The dashed curve represents 15% scaled down trend of $\text{As}_x\text{Se}_{1-x}$ molar volume data and represents approximately the predicted molar volumes of $\text{As}_x\text{S}_{1-x}$ glasses normalized for chalcogenide atom size. Note that the observed molar volumes are significantly higher than the predicted ones, suggesting $\text{As}_x\text{S}_{1-x}$ glasses to have much free volume, most likely coming from presence of non-bonding van der Waals interactions.

about 30 mg quantity of a sample, hermetically sealed in Al pans, was heated at a scan rate of 3 °C/min and a modulation rate of 1 °C/100 s. A scan up in temperature across T_g was then followed by a scan down in temperature. Scans of pure S and those of S-rich binary glasses at $x=8\%$ and 15% are reproduced in Fig. 5. In pure S [Fig. 5(a)], we observe three endothermic events: (i) an α - β solid-solid phase transformation near 108.6 °C, (ii) a melting of β -S near 118 °C, and followed by (iii) a T_λ transition near 160.6 °C. The T_λ transition is identified with opening of S_8 rings to form polymeric S chains leading to the formation of viscous or plastic S.⁵⁶ In the inset of Fig. 5(a), the scan of pure S is enlarged, and it highlights the nonreversing enthalpy associated with the T_λ transition, and one observes an endotherm exclusively. In S-rich glasses, and particularly at low x ($<23\%$), one observes in general, the total heat-flow scan to reveal two thermal events: a glass transition endotherm in the 20 °C $< T < 125$ °C range, followed by a complex heat-flow profile associated with the T_λ transition. Help in understanding the complicated total heat-flow profile comes from examining the deconvoluted reversing and nonreversing heat-flow profiles. In the reversing heat-flow scan, one observes a glass transition endotherm to display a rounded step in C_p , and one fixes the T_g value by the inflexion point of the step. The T_λ transition also displays a rounded step in C_p , and one fixes the transition temperature by the inflexion point of the step. The nonreversing heat flow, as expected, shows a Gaussian-type endotherm for the T_g event, but for the T_λ transition one observes an exotherm followed by an endotherm as illustrated in Figs. 5(b) and 5(c). These data suggest that as T increases, S_8 rings first become mobile near about 100 °C and coalesce to form nanocrystalline fragments, a process that releases heat (exotherm). With a further increase in T , these fragments dissociate and S_8 rings open and are incorporated in the backbone, events that contribute to the endotherm; and as the As content x of the glasses exceeds 15%, T_g 's steadily increase while the strength of the T_λ transitions

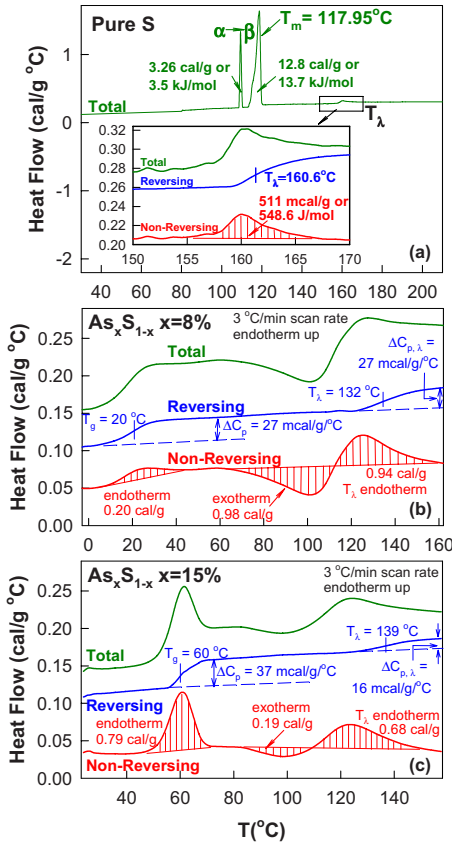


FIG. 5. (Color online) m-DSC scans of (a) orthorhombic sulfur, (b) As_8S_{92} glass, and (c) $\text{As}_{15}\text{S}_{85}$ glass. In (a) the three endothermic events, solid-solid phase transformation ($T_{\alpha \rightarrow \beta}$), melting transition (T_m), and sulfur polymerization transition (T_λ), are observed. In (b) and (c), the total (green), reversing (blue), and nonreversing (red) heat flows are shown. Notice that the nonreversing heat flow associated with the T_λ transition displays an exotherm followed by an endotherm in the glass samples but not in elemental sulfur. See text.

steadily diminishes as both ΔC_p and the nonreversing heat-flow term ΔH_{nr} decreases [Figs. 6(a) and 6(b)]. These data suggest that the process of alloying As in S leads to growth of network backbone as concentration of S_8 rings steadily decreases; and at $x > 25\%$, there is little or no evidence of S_8 rings present in glasses. Even in the most S-rich glass investigated here, we find no evidence of the $\alpha \rightarrow \beta$ transition as seen in pure S, suggesting that S_8 rings formed in our glass samples do “not” precipitate to form microcrystalline clusters of α -sulfur. These S_8 crowns, most likely, are randomly distributed with the network backbone. Trends in T_g for present $\text{As}_x\text{S}_{1-x}$ glasses appear in Fig. 7, where we show for comparison T_g 's in binary $\text{As}_x\text{Se}_{1-x}$ glasses. We shall discuss these results later.

In an m-DSC experiment, deconvolution of heat flow into a reversing and a nonreversing component has basic implications in understanding the nature of glass transition.³⁷ The former heat flow relates to ergodic events (vibrational entropy), while the latter to nonergodic events (configurational entropy) accompanying structural arrest near T_g . Data on chalcogenide glasses broadly reveal three generic types⁵⁷ of glass transitions based on connectivity of their backbones. Weakly cross-linked backbones form elastically flexible net-

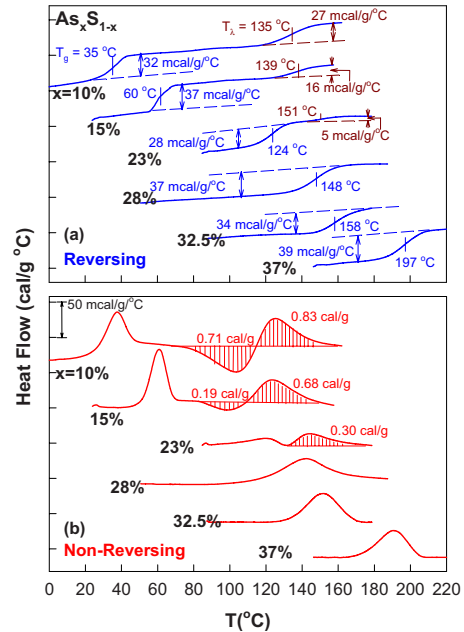


FIG. 6. (Color online) A summary of the (a) reversing heat-flow (blue) scans and (b) nonreversing heat-flow (red) scans at indicated As concentrations x in the As-S binary. Note that at $x > 23\%$, S_8 ring concentration nearly vanishes and only the glass transition endotherm is observed.

works, which display a nonreversing enthalpy at T_g , $\Delta H_{nr}(T)$, which is Gaussian-type, symmetric, and narrow ($\Delta T \sim 20^\circ\text{C}$) in width, and the term ages. Highly cross-linked backbones form elastically stressed-rigid networks, which display a $\Delta H_{nr}(T)$ term that is broad ($\Delta T \sim 40^\circ\text{C}$) and asymmetric with a high- T tail, and the term ages. On the other hand, optimally cross-linked backbones form elastically rigid but unstressed networks [intermediate phases (IPs)] which display a $\Delta H_{nr}(T)$ term that is not only minuscule but also does not age much. The vanishing of the ΔH_{nr} term for IP glass compositions suggests that such networks possess liq-

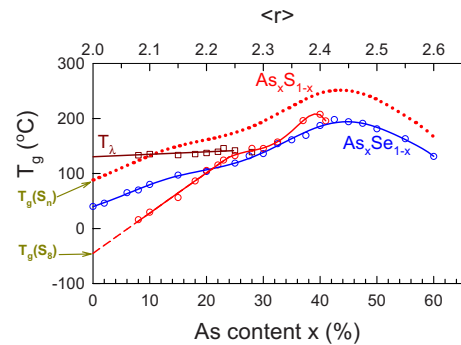


FIG. 7. (Color online) Variation in $T_g(x)$ in the present $\text{As}_x\text{S}_{1-x}$ binary (red) compared to the one in the $\text{As}_x\text{Se}_{1-x}$ binary (blue) [taken from Georgiev *et al.* (Ref. 19)]. Note the absence of chemical bond-strength scaling of T_g 's in the $25\% < x < 40\%$ range. The broken curve (.....) gives the expected T_g 's of the $\text{As}_x\text{S}_{1-x}$ glasses if S_8 rings had not decoupled from the glasses and bond-strength scaling had prevailed. The extrapolated $T_g(x=0)$ for a S_8 ring glass and a S_n chain glass are estimated at -50°C and about 95°C .

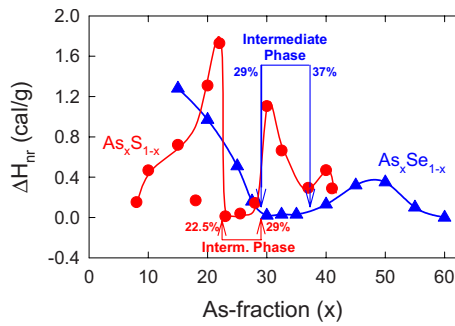


FIG. 8. (Color online) Reversibility windows in binary As–S (●, red) from the present work compared to the window in binary As–Se (▲, blue) taken from the work of Georgiev *et al.* (Ref. 19). Notice that the window centroid in the sulfide glasses is shifted to lower x in relation to the one in selenide glasses.

uidlike entropies, a feature that most likely derives⁵⁸ from presence of multiple isostatic local structures.

It is usual to make a frequency correction to the ΔH_{nr} term by subtracting the ΔH_{nr}^{cool} term measured in a cooling cycle from the ΔH_{nr}^{heat} term measured in the heating cycle;

$$\Delta H_{nr}^{freq.corr} = \Delta H_{nr}^{heat} - \Delta H_{nr}^{cool}. \quad (2)$$

The frequency corrected $\Delta H_{nr}^{freq.corr}$ term is independent of the modulation rate employed. Thus, for example, the ΔH_{nr}^{heat} and ΔH_{nr}^{cool} terms for a sample at $x=28\%$ are 0.86 and 0.73 cal/g, respectively, upon a frequency correction $\Delta H_{nr}^{freq.corr}$, which is found to be 0.13 cal/g (Fig. 8). The observed trends in non-reversing enthalpy reveal a narrow, deep and sharp reversibility window that onsets near $x=22.5\%$ and ends near $x=29\%$ (Fig. 8). For convenience, the reversibility window in As–Se glasses²² is also included in Fig. 8. We find the window in sulfide glasses is shifted to lower x in relation to the window in selenide glasses.

D. Raman scattering

Raman scattering was studied using a dispersive T64000 triple monochromator system from Horiba Jobin Yvon Inc., using 647 nm excitation. The dispersive system made use of a microscope attachment with an 80× objective, bringing laser light to a fine focus (2 μm spot size) and the scattered radiation detected using a charge-coupled device (CCD) detector. Samples in a platelet form were encapsulated in a MMR Joule-Thomson refrigerator to avoid photo-oxidation and heating. Spectra could be recorded from 3 to 600 cm⁻¹ range permitting the boson peak to be investigated. Typically 2 mW of laser power was brought on the microscope table over a 2 μm spot size. Separately samples were also studied using a Thermo-Nicolet FT-Raman system with 1.06 μm excitation from a Nd-doped yttrium aluminum (YAG) laser. The observed line shapes in either set looked very similar. In the FT-Raman experiments samples were encapsulated in evacuated quartz tubing and the laser beam of typically 260 mW power was brought to a loose focus (150 μm spot size) onto the samples. Figure 9 gives a summary of the observed line shape using an FT-Raman system for glass compositions in the 8% < x < 41% range. These results are quite similar to

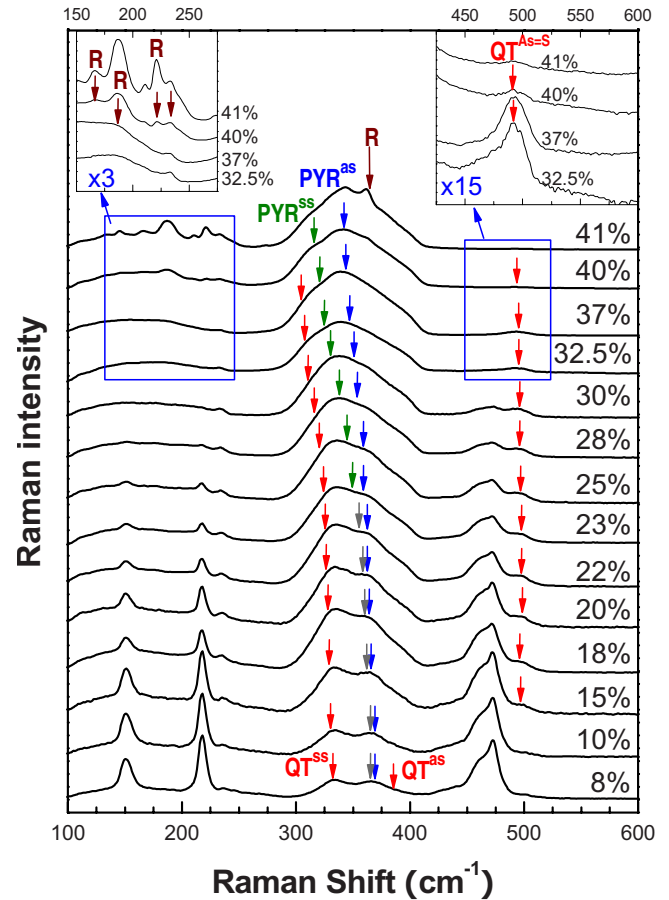


FIG. 9. (Color online) FT-Raman-scattering data on present As–S glasses at indicated glass compositions x on the right of each curve. Similar results have been reported by several other groups, such as Refs. 8, 11, 59, and 60. Near $x=40\%$, features of As_4S_4 molecules (labeled R for realgar) segregate from bulk glasses as shown in the left inset. Furthermore, a mode near 500 cm⁻¹, found to be present even at $x=41\%$, is shown in the right inset. PYR^{ss} and PYR^{as} represent the symmetric stretch and asymmetric stretch of pyramidal units. QT^{ss} and QT^{as} represent the symmetric stretch and asymmetric stretch of quasitrahedral units. $QT^{As=S}$ represents the stretch of the As=S double bond of QT units.

those reported earlier^{8,11,59,60} by several groups. At low x (<25%) one observes sharp modes that are readily identified with sulfur rings and chains. In the mid- x range (25% < x < 40%), the line shape is dominated by a broad band in the 300 < ν < 400 cm⁻¹ range. At high x (>40%), one begins to observe again some sharp features labeled as R in the spectra (Fig. 9). These R modes were identified earlier by Georgiev *et al.*²² as belonging to those of realgar (As_4S_4) molecules that demix from network structure once x exceeds 38%.

Guided by first-principles cluster calculations (Sec. III), we are now able to better decode the vibrational density of states and understand the structure consequences. The mid- x region is of interest, particularly since it is in this range one observes the reversibility window (RW). Examples of Raman line shape deconvolution for samples at $x=8\%$, 10%, and 15% appear in Fig. 10.

We concur with the earlier assignments⁶¹ of the narrow modes near 151 cm⁻¹ (S_8), 217 cm⁻¹ (S_8), 440 cm⁻¹

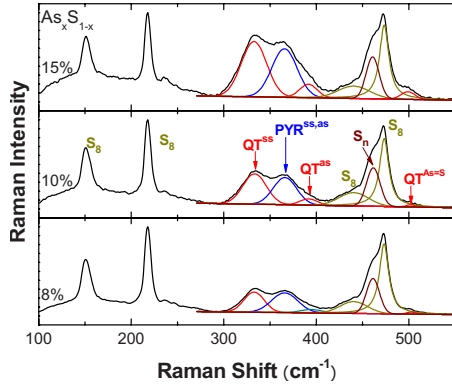


FIG. 10. (Color online) Line-shape analysis of Raman scattering in binary As–S glasses at indicated compositions, $x=8\%$, 10% , and 15% . The mode assignments are indicated in the middle panel. S_n : Sulfur chain mode; S_8 : sulfur ring modes. Also see Figs. 2 and 9 and Table I for mode identification.

(second-order scattering from 217 cm^{-1}), 461 cm^{-1} (S_n chains), and 474 cm^{-1} (S_8) as belonging to modes of either S_8 rings⁶¹ or S_n chains. The cluster calculations place the symmetric ($335^{\text{cal}}\text{ cm}^{-1}$) and asymmetric stretch ($365^{\text{cal}}\text{ cm}^{-1}$) of quasitetrahedral $\text{S}=\text{As}(\text{S}_{1/2})_3$ units (Table I). We thus assign the modes observed near 333 and 380 cm^{-1} , respectively, to these vibrational modes of QT units. The $\text{As}=\text{S}$ stretch mode of such a unit we believe contributes to the mode near 500 cm^{-1} in the spectra (Table I). The cluster calculations place the symmetric ($352^{\text{cal}}\text{ cm}^{-1}$) and asymmetric ($355^{\text{cal}}\text{ cm}^{-1}$) stretches of pyramidal $\text{As}(\text{S}_{1/2})_3$ units quite close to each other, and we assign the feature observed near 365 cm^{-1} to both these vibrational modes.

The observed FT-Raman line shapes in the $250\text{--}550\text{ cm}^{-1}$ range were fitted using a least-squares routine to a superposition of several peaks. Gaussian profiles were used in general, except for the sharper S_8 ring modes where a Voigt or Gaussian-Lorentzian profile worked better. Examples of line-shape fits at $x=8\%$, 10% , and 15% appear in Fig. 10.

From these fits, we have also extracted the normalized scattering strength (A_n/A) of the modes at $\nu_1=333\text{ cm}^{-1}$ (QT^{ss}), $\nu_2=365\text{ cm}^{-1}$ (PYR), and $\nu_3=495\text{ cm}^{-1}$ (QT) and Fig. 11 gives a plot of the compositional trends of mode scattering strengths. The total integrated area A under the various modes was used to normalize the individual mode scattering strengths. As expected, modes assigned to S chains (461 cm^{-1}) and rings (474 cm^{-1}) monotonically decrease in scattering strength to nearly vanish as x increases to 40% . On the other hand, modes assigned to QT units (333 and 495 cm^{-1}) show a global maximum in the ($22\text{--}29\%$) range, compositions belonging to the RW. The scattering strength of the mode near 365 cm^{-1} assigned to PYR units is found to increase monotonically as x approaches 40% with a mild plateau in the RW range. We consider these compositional trends in scattering strengths of Raman modes to be more compelling than the mode frequencies alone in making local structure assignments, and this is a point we shall return to discuss later. Figure 12 summarizes the glass composition

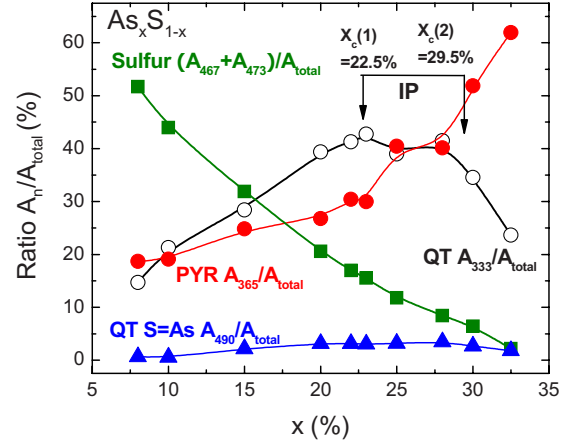


FIG. 11. (Color online) Variations in Raman mode normalized scattering strengths (A_n/A_{tot}) as a function of glass compositions x in the present $\text{As}_x\text{S}_{1-x}$ binary: sulfur chain and ring modes (■, green) at 467 and 473 cm^{-1} , QT mode (○) at 333 cm^{-1} , QT mode (▲, blue) at 490 cm^{-1} , and PYR mode (●, red) at 365 cm^{-1} . Vibrational mode strengths were normalized to the total area under various modes. Note that the two QT modes (○ and ▲) show a broad global maximum in the IP.

dependence of the Raman-active bond-stretching mode frequencies due to QT and PYR units. One finds that in the $10\% < x < 30\%$ range mode frequencies steadily redshift by nearly 15 cm^{-1} . This is unusual, and we shall comment on the behavior in Sec. V.

In the observed line shapes, scattering in the low-frequency range increases remarkably as the As content of glasses $x < 20\%$ as illustrated in Fig. 13, which gives the dispersive Raman spectra. In making these plots we have normalized the observed spectra to the same laser power and find that compositional trends in scattering strength of modes in the bond-stretching regime [S_8 ring bond-bending mode (at 217 cm^{-1})] and the stretching mode of PYR units (at 365 cm^{-1} and stretching modes of QT units) monotonically

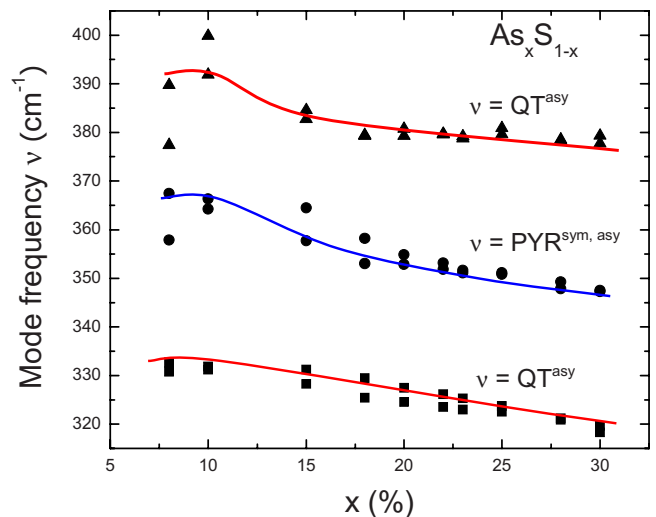


FIG. 12. (Color online) Compositional trends in Raman mode frequency of characteristic vibrational modes of QT and PYR units showing a redshift with increasing x .

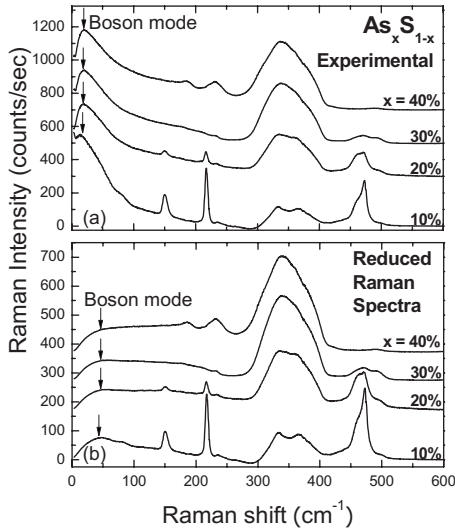


FIG. 13. Dispersive Raman spectra of $\text{As}_x\text{S}_{1-x}$ glasses showing the boson mode at low frequencies at indicated compositions x on the right in percent: (a) observed Raman spectra (I_{expt}) and (b) reduced Raman spectra $\{I_{\text{expt}}/[n_B+1]\}$. Here n_B is the Bose occupation number. Note that the boson mode is the most important feature of the spectra in (a). In the reduced Raman spectra (b) the skewed line shape at low frequency due to the finite T is removed, and the peak shifts up in frequency.

change with glass composition x as expected. To better visualize these excitations, we present in Fig. 13, the experimental (I_{expt}) Raman line shapes along with reduced Raman vibrational density of states (I_{red}) at several compositions. These data demonstrate that low-frequency vibrational modes “dominate” Raman scattering (Fig. 13) in the present sulfides at low x , and particularly at $x < 20\%$, a feature that was also noted by earlier workers in the field.⁶⁰ The boson mode in As_2S_3 glass was also observed in IR transmission experiments.⁶²

Raman scattering can, in general, be written⁶³ as follows:

$$I_{\text{expt}} \sim C(\omega)g(\omega)[n_B + 1]/\omega, \quad (3)$$

where n_B represents the Bose occupation number, $C(\omega)$ is the photon-vibration coupling constant, and $g(\omega)$ is the vibrational density of states (VDOS). To obtain the excess VDOS (e-VDOS) over Debye-type vibrations, we follow the following procedure.⁶⁴ From the observed Raman scattering I_{expt} , we obtain the reduced Raman VDOS

$$I_{\text{red}} = I_{\text{expt}}/(n_B + 1) \quad (4)$$

and subtract an estimated Debye-type density of states to obtain e-VDOS, as illustrated for two glass compositions at $x=10\%$ and 40% in Fig. 14. In estimating the Debye density of states we scale the slopes of these curves as $1/v^3$, where v is the speed of sound.⁶⁵ The resulting e-VDOSs are illustrated as the crosshatched region in Fig. 14. A plot of the peak frequency, $\nu_{\text{e-VDOS}}$ and integrated intensity, $I_{\text{e-VDOS}}$ of the e-VDOS appears in Figs. 15(a) and 15(b), respectively. One finds that $\nu_{\text{e-VDOS}}(x)$ [Fig. 15(a)] smoothly increases from a value of 42 cm^{-1} at $x=8\%$ to 48 cm^{-1} at $x=41\%$, but with a local minimum in frequency near $x=25\%$ in the re-

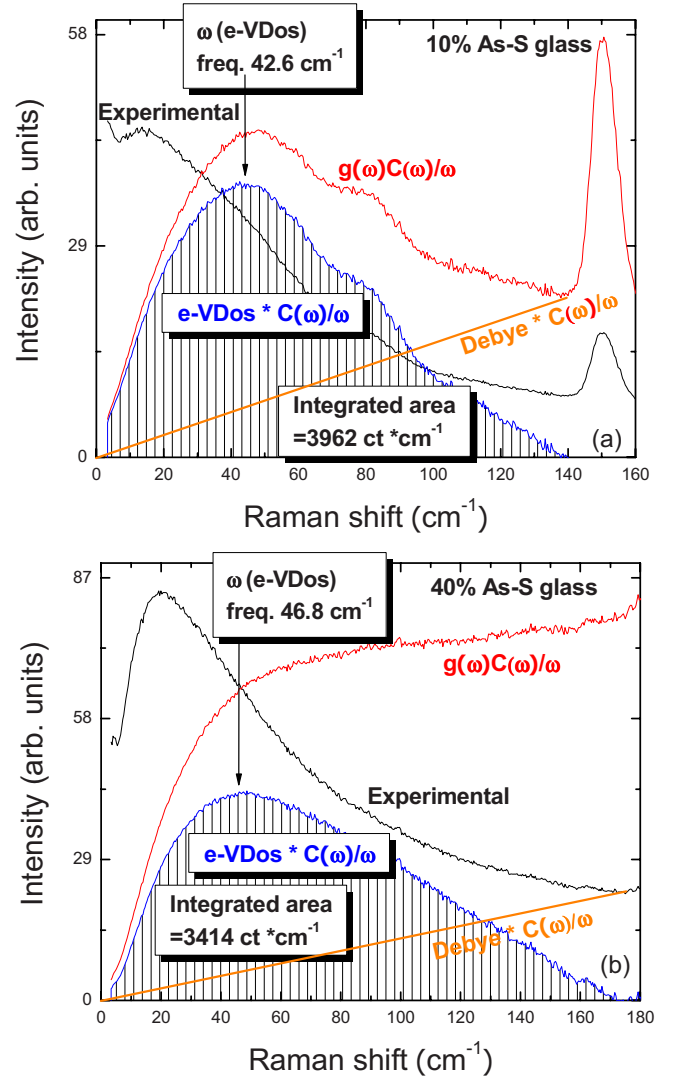


FIG. 14. (Color online) Deconvolution of the reduced Raman spectra (red) $[g(\omega)C(\omega)/\omega]$ at two compositions, (a) $x=10\%$ (top panel) and (b) $x=40\%$ (bottom panel), showing extraction of the excess vibrational density of states, e-VDOS (blue), by subtracting a Debye-type term (orange) from the total scattering.

versibility window. On the other hand, $I_{\text{e-VDOS}}(x)$ remains largely unchanged in the $41\% < x < 20\%$ range but increases almost linearly in the $20\% < x < 8\%$ range. We shall return to discuss these results in Sec. V.

E. IR reflectance

A Thermo-Nicolet model FTIR model 870 with a smart collector accessory was used to examine specular reflectance data from polished platelets of $\text{As}_x\text{S}_{1-x}$ glass samples. Typical sample size used was 5 mm in diameter and 2 mm in thickness. Reflectivity was studied over the $50\text{--}600 \text{ cm}^{-1}$ range using solid-state substrate beam splitter and DTGS detector with polyethylene window. A typical measurement used 600 scans with a 12 min scan time to give 4 cm^{-1} resolution. A polished stainless-steel surface was used as a reference for normalization of reflectivity. A Kramers-Kronig

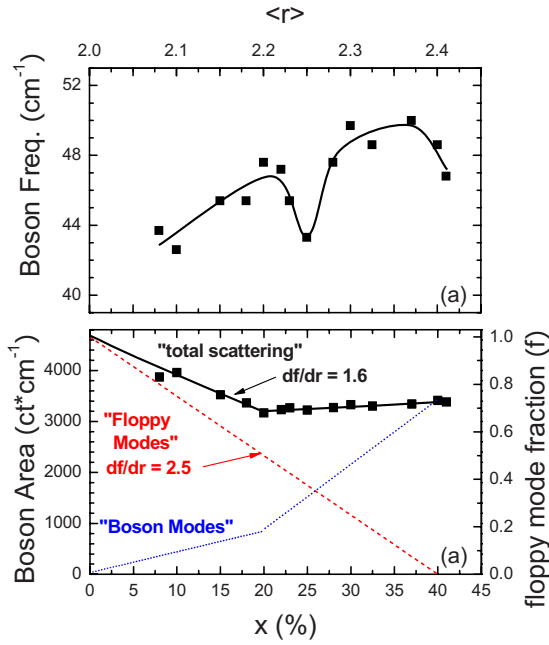


FIG. 15. (Color online) Variations in (a) the boson mode frequency (■) and (b) boson mode integrated intensity (■) as a function of glass composition x in As_xS_{1-x} binary. In (b), the - - - line gives the floppy mode variation with $r=2+x$ and the ···· line gives the difference between the integrated intensity (■) and the floppy mode (- - -) contribution.

transformation of the reflectance signal was performed with GRAMS software to generate absorbance and transverse-optic (TO) and longitudinal-optic (LO) IR responses.

A summary of the reflectance signal data recorded at several glass compositions appears in Fig. 16(a). These data are quite similar to the ones reported earlier.¹¹ The IR TO (ϵ_2) response for glasses is summarized in Fig. 16(b) and is found to be quite similar to those reported earlier.¹¹ We have sum-

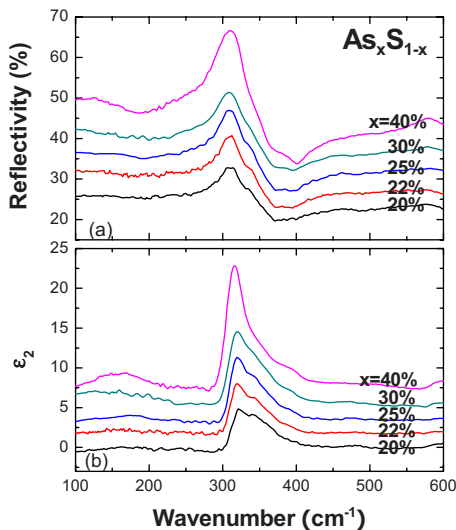


FIG. 16. (Color online) (a) Observed IR reflectance and (b) the imaginary part of dielectric constant ϵ_2 (TO response) in binary As_xS_{1-x} glasses. The TO response was deduced from Kramers-Kronig transformation of the reflectance data.

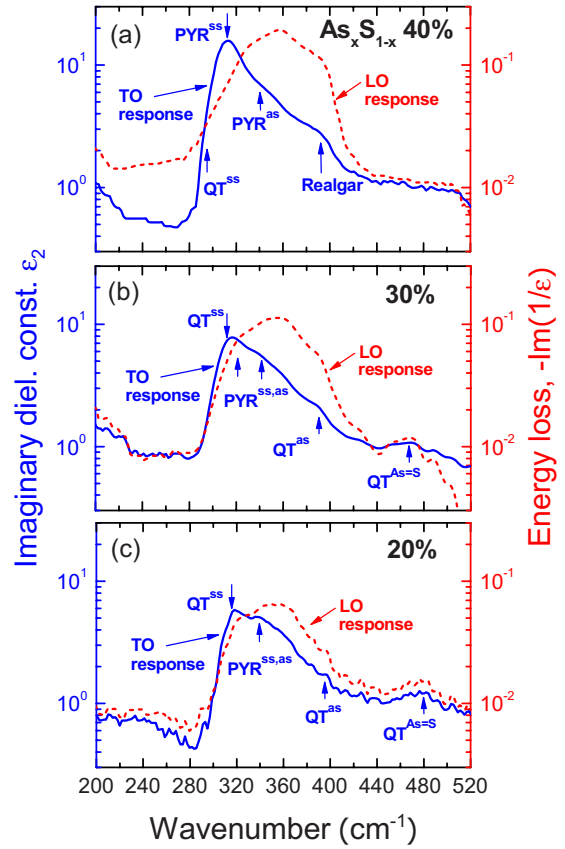


FIG. 17. (Color online) Infrared transverse-optic TO (blue) and longitudinal optic LO (red) responses at select As_xS_{1-x} glass compositions, (a) $x=40\%$, (b) $x=30\%$, and (c) $x=20\%$ compared. See text for details.

marized the TO as well as the LO response at select glass compositions (20%, 30%, and 40%) in Fig. 17. The data for the stoichiometric composition, $x=40\%$, may be compared to those of earlier reports.^{11,12} In these data one can see vibrational features near 312 cm⁻¹ and near 340 cm⁻¹ identified earlier¹² with the symmetric and asymmetric stretches of PYR units. In addition there are other features present in these data, which make the IR response consistent with the present and earlier²² Raman data. For example, network modes of PYR units²² must also contribute to the IR response particularly in the 360–400 cm⁻¹ range. In this range, the presence of realgar units (As_4S_4) in the As_2S_3 glass, noted earlier in Raman scattering, will also contribute to (features near 300 and 370 cm⁻¹) in the IR response. Mori *et al.*¹¹ observed a small but clearly resolved feature near 490 cm⁻¹ in the IR absorption measurements of the stoichiometric glass ($x=40\%$). The feature comes from the stretch of As=S double bonds of QT units. The broad TO response observed in the 280–500 cm⁻¹ range (Fig. 17) must then also include features from the symmetric and asymmetric stretches of the QT units.

In a glass of composition $x=30\%$, Raman scattering reveals no evidence of realgar units. In the IR response one thus expects contributions from both PYR and QT units as shown in the middle panel of Fig. 17(b). At $x=20\%$, Raman scattering reveals significant contribution from S_n chains and

S_8 rings. One thus expects, in addition to modes of QT and PYR units, those of S_n chains and rings to contribute to the IR response near 480 cm^{-1} . One can see evidence of some IR response in the $440\text{--}500\text{ cm}^{-1}$ range in the data of Fig. 17(c). Unlike Raman modes that are reasonably sharp, the IR response from these glasses reveals modes that are quite broad, and a unique deconvolution of the observed line shape becomes more challenging. Finally, a perusal of the data of Fig. 17 illustrates the LO response to be shifted to higher frequency in relation to the TO response. In polar semiconductors internal electric fields add to the external one and blueshift the LO response to higher frequencies in relation to the TO response, as expected.

V. DISCUSSION

A. Identification of the three elastic phases in binary As_xS_{1-x} glasses

RWs have been observed in chalcogenides^{18,19,43,66,67} and more recently in oxide glasses⁶⁸ as well. These windows are identified with glass compositions belonging to an IP bordered on the low connectivity end by a flexible phase and on the high connectivity end by a stressed-rigid phase. Glass compositions in these windows form networks that are rigid but unstressed. Material compositions in the IP are functionally quite different from those in the flexible or stressed-rigid phases; they age minimally and display dynamic reversibility and have often been compared to proteins in the transition state that fold reversibly. These features of the IP are reviewed as representing a self-organized^{69–72} phase of disordered matter.

In Fig. 18, we have assembled the compositional variation in $T_g(x)$, nonreversing enthalpy $\Delta H_{nr}(x)$, and molar volumes $V_m(x)$ in the present binary glasses. The minuscule $\Delta H_{nr}(x)$, in the $22.5\% < x < 29.5\%$ range, serves to define the RW in the present glasses. In analogy to earlier work on chalcogenides, we identify the RW with the IP of the present glasses. The variation in molar volumes reveals an almost linear decrease in the $10\% < x < 40\%$ range, but with some evidence of a “local minimum” in the RW (Fig. 18), which is surely the signature of space filling of the IP. Identification of the IP thus permits fixing the three elastic regimes in the present binary glasses. Compositions at $x < 22.5\%$ belong to the elastically flexible phase, while those on the high connectivity end at $x > 29.5\%$ to the elastically stressed-rigid phase. The stoichiometric glass composition, As_2S_3 ($x = 40\%$) is found not to be a part of the IP.

In the flexible phase of the present sulfides networks rapidly segregate as the As concentration decreases from 20% to 8% range. The almost linear reduction in $T_g(x)$ at $x < 22\%$ [Fig. 18(a)], the increase in concentration of S_8 rings as reflected in growth in scattering strength of 217 cm^{-1} (bending mode of S_8 rings) in Raman scattering [Figs. 9 and 18(a)], and the appearance of the T_λ transition in calorimetry, each of the data corroborates the general picture of S_8 crowns demixing from the backbone of glasses in the flexible phase; but even at the lowest As concentration examined here, we

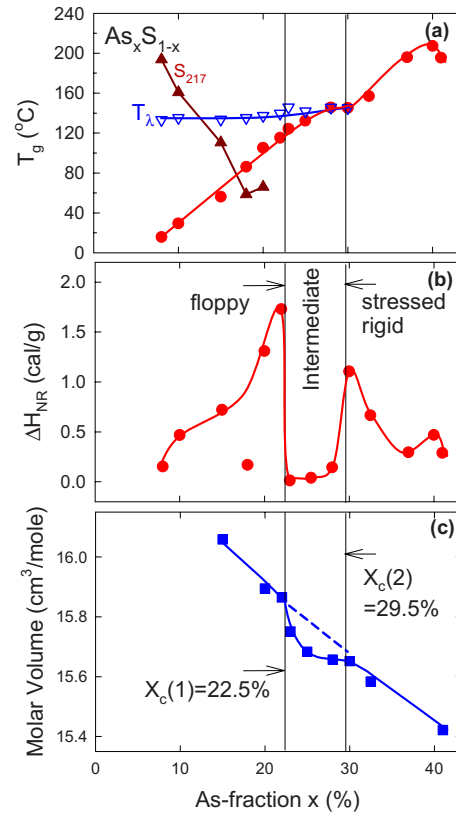


FIG. 18. (Color online) Compositional trends in (a) $T_g(x)$ (●, red), $T_\lambda(x)$ (△, blue), and the sulfur ring Raman mode near 217 cm^{-1} (▲, red), (b) nonreversing enthalpy $\Delta H_{nr}(x)$ (●, red) (■, blue), and (c) molar volumes (■, blue) of binary As–S glasses from the present work. The reversibility window is observed in the $22.5\% < x < 29.5\%$ range, an observation that fixes the intermediate phase in the present sulfides. Also note that molar volumes show a local minimum in the IP.

could not detect S_8 crowns segregating to form the crystalline orthorhombic S phase; there is no evidence of the $\alpha \rightarrow \beta$ transition in calorimetry (Fig. 5). In the IP, and particularly in $22.5\% < x < 25\%$ range, there is evidence of a small (2%) but decreasing concentration of S_8 rings present as x increases to about 25%.

In the stressed-rigid phase, one finds $T_g(x)$ to increase with x , which is consistent with PYR and QT units serving to cross-link S_n chain segments and increasing connectivity of networks. The concentration of both PYR units increases with x in the $29\% < x < 40\%$ range. In spite of this trend, Raman vibrational mode frequencies of the two building blocks are found not to increase. These data suggest that the PYR and QT units and S_n chains must not form part of the same fully polymerized structure as has been traditionally assumed. In several binary^{66,73} and ternary^{67,74} selenides that usually form fully polymerized networks, Raman-scattering-derived optical elastic constants (or mode frequency squared) display an increase as a power law with glass composition x in the stressed-rigid phase. The absence of such a power-law variation underscores that underlying networks of the present sulfides are most likely not fully connected by covalent bonds alone (see below).

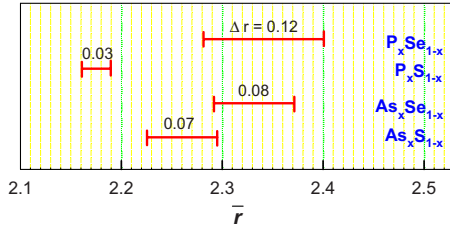


FIG. 19. (Color online) Observed IPs in group-V chalcogenides. The bar chart gives the mean coordination number interval, Δr , across which IPs extend as noted by reversibility windows in m-DSC experiments.

B. Local structures of binary As_xS_{1-x} glasses and the intermediate phase

Identification of the three elastic phases in the present binary begs the broader issue—what aspects of glass molecular structure control their elastic behavior? In particular, can one understand the width and centroid of the IP in the present binary sulfides? Several numerical approaches to model IPs (Refs. 69–72) in the selenides have been discussed recently. In the sulfides that intrinsically segregate on nanoscale, experiments can however provide crucial insights on these phase-separation effects, and such effects are likely to serve as important bounds in modeling IPs as well.

The IP in the present sulfides ($22.5\% < x < 29.5\%$) is shifted to a lower range of x in relation to corresponding selenides ($28\% < x < 37\%$), as shown in Fig. 8. To put these results in perspective, we have compared known IPs in group-V sulfides with corresponding selenides²¹ in Fig. 19. The IP in P–Se and As–Se binary systems display close parallels; their centroids are nearly the same, although IP width of the P–Se binary ($\Delta r=0.12$) exceeds that of the As–Se ($\Delta r=0.08$) one. We believe that aspects of local structure, directly accessible from experiments, most likely play a role in determining these widths. There are two local structures, PYR ($r=2.40$) and QT units ($r=2.28$), in As–Se glasses that contribute to the width of the IP. On the other hand, there are three local structures that contribute to the IP width in P–Se glasses: PYR ($r=2.40$), QT ($r=2.28$), and a polymeric ethylenelike (ETY) P_4Se_4 unit ($r=2.5$). The number appearing in parentheses describes the mean coordination number of these units or chemical stoichiometry. While the PYR and QT units are isostatic, the ETY units are mildly stressed rigid. The somewhat larger width of the IP in P–Se glasses than in As–Se ones, most likely, derives from the wider range in r spanned by the three local structures. On the other hand, the similarity of IP centroids comes largely from the fact that both these group-V selenides form polymerized network structures in which Se_n chains are part of the network backbone (Fig. 19).

Moving next to the cases of the binary As and the P sulfides, one is struck by the shift of IP centroids to lower x in relation to corresponding selenides (Fig. 19). What aspect of glass structure contributes to the shift? It is instructive to first consider the case of P–S binary, where there is recognition²¹ that the IP centroid shift to lower x results from a complete segregation of the excess S_n chain fragments from the PYR and QT units bearing connective tissue (backbone). In Ra-

man scattering, vibrational modes of QT, PYR, and S_n chains are completely resolved²¹ in binary P–S glasses. The concentrations of these local structures can then be estimated, and one finds that the chemical stoichiometry of the IP backbone equals $P_{33}S_{66}$ if all excess S is to completely segregate from the backbone. On the other hand, in P–Se glasses IP centroid stoichiometry, $[x_c(1)+x_c(2)]/2=[29\%+37\%]/2$ also equals 33%, the same value as found in P–S glasses. We are thus led to think that the IP centroid shift in P–S glasses is largely a manifestation of the excess S (as S_n chain fragments) completely decoupling from the backbone.

A perusal of the data of Fig. 19 also shows that the IP centroid in binary As–S glasses is shifted halfway between the case of P–Se (Se_n chains fully coupled to network) and that of P–S (S_n chains fully decoupled from the network) glasses. Thus, a plausible explanation is that about half of the excess S forms part of the backbone while the other half is decoupled from the backbone in binary As–S glasses. The demixed excess S cannot be present in short (<8 atom long) S_n chain fragments; otherwise, one would have seen end effects. The demixed S_n chains are most likely at least 15 atoms or longer. To put the number in perspective, Kozhevnikov *et al.*⁷⁵ in their studies of the depolymerization transition in elemental sulfur placed the length of sulfur chains close to 100 nm long or about 600 atoms long. The excess S in the IP is viewed as present in chains (and not rings) as suggested by Raman scattering (Fig. 9).

What can we say about the width of the IPs in the sulfide glasses? For the companion binary P–S glasses, an IP is observed in the $16\% < x < 19\%$ range ($\Delta r=0.03$), and one finds QT units and PYR units concentrations to show global maxima, respectively, at the lower end ($x=16\%$) and at the upper end ($x=19\%$) of that phase. We believe that a parallel circumstance prevails in the As–S binary with both PYR and QT units contributing to the width of the IP. We have already noted that QT unit concentrations display a maximum in the IP (Fig. 11). On the other hand, PYR unit concentration increases monotonically with x to maximize near $x=40\%$ in the As–S binary (Fig. 11). This particular feature of the data on As–S glasses differs from the case of the P–S glasses in large part because P–P bonds (51.3 kcal/mol) have a higher chemical bond strength than As–As (32.1 kcal/mol) bonds, and these bonds readily are manifested in P_4S_{10} molecules that decouple from the backbone just above the IP.²¹

Nanoscale phase-separation effects, such as formation of small molecules that demix from a backbone, result in loss of network character, a structural feature that plays an important part in determining IP widths in glasses. We have already noted^{21,34} that segregation of S_8 rings at low x ($<14\%$) and of P_4S_{10} molecules at high x ($>20\%$) serves to restrict the range of glass formation, and the IP as well. Parallel considerations must also apply to the case of the present As_xS_{1-x} binary, wherein at $x < 18\%$ concentration of S_8 rings proliferate while at $x > 38\%$, As_4S_4 molecules decouple²² from the network. In fact bulk glass formation in the As–S binary ceases at $x > 50\%$ largely because of the preponderance of As_4S_4 molecules in melts, which upon cooling give rise to the crystalline phase, realgar.⁷⁶ IPs in network forming systems require that there be a significant fraction of the connective tissue present for a glass network to form an IP and self-organize.

The broad picture of partial demixing of S_n chains in the IP of As–S glasses described above is corroborated by molar volumes and T_g 's of glasses. Partial demixing of S_n chains from network backbone contributes to the increased free volume of As–S glasses (Fig. 4) as discussed earlier in Sec. IV. The almost complete absence of chemical bond-strength scaling of T_g 's between As–Se and As–S glasses, and also in the IP (Fig. 7), is suggestive that network connectivity of sulfide glasses is “lower” than of the counterpart selenides. In summary, the shift of the IP to lower x , the increased molar volumes, and the complete absence of bond-strength scaling of T_g 's in the As–S glasses in relation to As–Se glasses, each point to the partial demixing of S_n chain fragments from network backbone.

C. Low-frequency vibrational modes: Evidence of boson and floppy modes

An almost universal feature of disordered solids is the appearance of vibrational modes at low frequency (5–60 cm^{-1} range) in Raman scattering, inelastic neutron scattering, and low-temperature specific heats broadly known as “boson modes.” These modes are identified with an excess of vibrations over Debye-type ones [$g(\nu) \sim \nu^2$] and probably come from some transfer of strength from high to low frequencies as an ordered crystalline solid is rendered disordered amorphous. The nature of these excess vibrations has been a subject of ongoing debate over the past 2 decades or more.^{77–79} Most work on boson modes has been performed on stoichiometric glasses and polymers, and in some cases the role of temperature and pressure⁸⁰ has also been investigated. In select cases compositional studies on glasses have also been performed.⁸¹ Recently, attention has been paid to analysis of low-frequency Raman modes to extract meaningful boson parameters from the e-VDOS that could be related to other probes of these vibrations.

In the present work we have paid particular attention to analyzing the low-frequency Raman-scattering data over a wide range of compositions ($8 < x < 41\%$) encompassing the flexible, intermediate, and the stressed-rigid phases of $\text{As}_x\text{S}_{1-x}$ glasses. Details of the analysis were presented in Sec. IV. Perusal of the data of Fig. 15(b) shows that the slope of the normalized integrated intensity $I_{e\text{-VDOS}}/I_{e\text{-VDOS}}(x=0)$ with x yields a value of the slope, $d[I_{e\text{-VDOS}}/I_{e\text{-VDOS}}(x=0)]/dx=1.6(1)$. The result is reminiscent of the floppy mode fraction change with r in rigidity theory.¹⁶ In a three-dimensional (3D) network of chains or rings, wherein each atom has two near neighbors, or $r=2$, there is one floppy mode ($f=1$) per atom. Upon alloying As with S, the resulting glass network becomes increasingly cross-linked as the mean coordination number, $r=2+x$, increases, and the floppy mode count $f(r)$ steadily decreases,

$$f = 6 - (5/2)r \quad (5)$$

and as x approaches 40%, or $r=2.40$, networks become rigid. In such a mean-field description of the onset of rigidity, one finds that the slope, $df/dr=2.50$ (Eq. (5)). Given that $r=2+x$, the observed slope as a function of r , also represents the slope as a function of x ; since $d[I_{e\text{-VDOS}}/I_{e\text{-VDOS}}(x=0)]/dr$

$=d[I_{e\text{-VDOS}}/I_{e\text{-VDOS}}(x=0)]/dx=1.6(1)$. In other words, the observed variation in the integrated intensity of the low-frequency modes as a function of r in our experiments of 1.6 is somewhat lower than the rigidity theory prediction of the slope of 2.5.

The most natural interpretation of these data is that the low-frequency vibration modes in these glasses have contributions arising from two sources: (i) floppy modes associated with the twofold coordinated S atoms in rings and chains and (ii) soft modes associated with a domain structure of glasses [Fig. 15(b)]. The latter modes were discussed by Duval *et al.*,⁷⁷ who suggested that glasses may be visualized as composed of a domain structure, with domains representing nanometer-sized elastically stiff regions in which atoms are strongly bonded and move together as a unit against other domains. The boson mode is viewed as an interdomain soft acoustic vibration, and its frequency is given by

$$\omega = v_s/2cR, \quad (6)$$

where v_s , c , and R represent, respectively, the velocity of sound, velocity of light, and the mean size of a domain. Taking velocity of sound in pure S to be 1250 m/s (Ref. 75) at 196 °C and of As_2S_3 glass to be 2100 m/s,⁸² we have interpolated the speed of sound for intermediate compositions. The domain size, R , suggested from Eq. (5), is then found to increase monotonically from 0.55 nm near $x=5\%$ to 0.75 nm near $x=45\%$. The trend of an increase in R with x appears quite plausible given that binary glasses become more connected, although it is at present less clear if the magnitude of R can be identified with characteristic clusters in these glasses.

The reversibility window in the present glasses shows that the rigidity transition in the present glasses occurs near $x=22\%$ [window onset composition $x_c(1)$] and the stress transition near 30% [window end composition, $x_c(2)$]. Within a mean-field description one expects the floppy mode contribution $f(x)$ to nearly vanish as x increases to 22%. Thus, a possible description of the low-frequency vibrations in these glasses is that [Fig. 15(b)] these are dominated by floppy modes at low x , and soft modes at high x . The soft or boson mode contribution most likely comes from the intrinsically heterogeneous character of the present sulfide glasses resulting from the partially polymerized nature of the backbone structure. Structural groupings such as S_8 rings and S_n chain fragments that decouple from the network backbone will contribute to the soft-mode behavior.

The onset of the flexible phase at $x < 22.5\%$ signaled by the calorimetric measurements, and the growth in low-frequency vibrations in Raman scattering at $x < 20\%$, is a striking result. These findings illustrate that two completely independent probes, light scattering and calorimetry, come together in quantitatively probing the flexible phase of the present glasses in a rather convincing fashion. The Raman and calorimetric data on the present glasses quantitatively connects boson modes and floppy modes to the low-frequency vibrations observed in a network glass.

VI. CONCLUSIONS

Dry and homogeneous bulk $\text{As}_x\text{S}_{1-x}$ glasses, synthesized over the $8\% < x < 41\%$ range, were investigated in modulated DSC, Raman scattering, infrared reflectance, and molar volume measurements. The following conclusions emerge from this work. (a) Vibrational mode assignments, assisted by first-principles cluster calculations, have permitted decoding aspects of local structures and show that both pyramidal $\text{As}(\text{S}_{1/2})_3$ and quasitetrahedral $\text{S}=\text{As}(\text{S}_{1/2})_3$ local structures are formed in these glasses. (b) Modulated DSC experiments reveal existence of a reversibility window in the $22.5\% < x < 29.5\%$ range that is identified with IP, with glasses at $x < 22.5\%$ in the flexible phase and those at $x > 29.5\%$ in the stressed-rigid phase of the present As sulfides. (c) Molar volumes of the glasses decrease almost linearly with increasing x displaying a local minimum in the IP. (d) The shift of the IP centroid in the present As sulfides to lower As concentration x compared to the IP in corresponding As selenides is identified with nearly half of the excess sulfur decoupling from the backbone in the present sulfides in contrast to all excess Se forming part of the network backbone in corresponding As selenides. (e) The presence of both pyramidal

$\text{As}(\text{S}_{1/2})_3$ and quasitetrahedral $\text{S}=\text{As}(\text{S}_{1/2})_3$ local structures as building blocks of these glasses provide the structural variability to understand the width of the IP qualitatively, with the QT units contributing to the lower end and PYR units to the upper end of the window. (f) Low-frequency Raman modes, generally identified as boson modes, increase in scattering strength linearly as As content x of glasses decreases from $x=20\%$ to 8% , with a slope that is close to the floppy mode fraction in flexible glasses predicted by rigidity theory. The result shows that floppy modes contribute to boson modes in flexible glasses. In the intermediate and stressed-rigid elastic phases, scattering strength of boson modes persist at a constant level, a finding we attribute to the presence of soft modes associated with domain structure of glasses. Both floppy modes and soft modes contribute to boson modes in the present glasses.

ACKNOWLEDGMENTS

It is a pleasure to acknowledge discussions with Bernard Goodman, Eugene Duval, and Darl McDaniel during the course of this work. This work is supported by NSF Grant No. DMR 04- 56472 to University of Cincinnati.

-
- ¹M. Mitkova, Y. Wang, and P. Boolchand, *Phys. Rev. Lett.* **83**, 3848 (1999).
²M. N. Kozicki and W. C. West, U.S. Patent No. 5,896,312 (20 April 1999).
³M. N. Kozicki, M. Park, and M. Mitkova, *IEEE Trans. Nanotechnol.* **4**, 331 (2005).
⁴P. Boolchand and W. J. Bresser, *Nature (London)* **410**, 1070 (2001).
⁵C. Holbrook, P. Boolchand, P. Chen, A. Pradel, and A. Piarristeguy, *Bull. Am. Phys. Soc.* **53**, 927 (2008).
⁶V. Balan, A. Piarristeguy, M. Ramonda, A. Pradel, and M. Ribes, *J. Optoelectron. Adv. Mater.* **8**, 2112 (2006).
⁷M. Kincl and L. Tichý, *Mater. Chem. Phys.* **103**, 78 (2007).
⁸T. Wagner, S. O. Kasap, M. Vlcek, A. Sklenar, and A. Stronski, *J. Mater. Sci.* **33**, 5581 (1998).
⁹K. Tanaka, *Phys. Rev. B* **36**, 9746 (1987).
¹⁰K. Shimakawa, A. Kolobov, and S. R. Elliott, *Adv. Phys.* **44**, 475 (1995).
¹¹T. Mori, K. Matsuishi, and T. Arai, *J. Non-Cryst. Solids* **65**, 269 (1984).
¹²G. Lucovsky, *Phys. Rev. B* **6**, 1480 (1972).
¹³A. T. Ward, *J. Phys. Chem.* **72**, 4133 (1968).
¹⁴C. Y. Yang, M. A. Paesler, and D. E. Sayers, *Phys. Rev. B* **39**, 10342 (1989).
¹⁵J. C. Phillips, *J. Non-Cryst. Solids* **34**, 153 (1979).
¹⁶M. F. Thorpe, *J. Non-Cryst. Solids* **57**, 355 (1983).
¹⁷For an atom possessing a coordination of r , in three dimensions there are $r/2$ bond-stretching and $(2r-3)$ bond-bending constraints per atom. For a PYR unit, $\text{As}(\text{Se}_{1/2})_3$, As is threefold ($r=3$) and Se is twofold ($r=2$) coordinated. The count of constraints for As is 4.5 and for Se is 2. The count of constraints per atom for a PYR unit then becomes $n_c=(4+3 \times 2 \times 1/2)/2.5=7.5/2.5=3$.
¹⁸P. Boolchand, G. Lucovsky, J. C. Phillips, and M. F. Thorpe, *Philos. Mag.* **85**, 3823 (2005).
¹⁹D. G. Georgiev, P. Boolchand, and M. Micoulaut, *Phys. Rev. B* **62**, R9228 (2000).
²⁰M. Micoulaut, *Eur. Phys. J. B* **1**, 277 (1998).
²¹P. Boolchand, P. Chen, and U. Vempati, arXiv:0809.1469, *J. Non-Cryst. Solids* (to be published).
²²D. G. Georgiev, P. Boolchand, and K. A. Jackson, *Philos. Mag.* **83**, 2941 (2003).
²³L. Pauling, *The Nature of the Chemical Bond* (Cornell University, Ithaca, NY, 1960).
²⁴V. F. Kokorina, *Glasses for Infrared Optics* (CRC, Boca Raton, FL, 1996).
²⁵M. Yamane and Y. Asahara, *Glasses for Photonics* (Cambridge University Press, Cambridge, England, 2000).
²⁶M. Munzar and L. Tichý, *J. Mater. Sci.: Mater. Electron.* **18**, 251 (2007).
²⁷J. M. Harbold, F. Ilday, F. W. Wise, J. S. Sanghera, V. Q. Nguyen, L. B. Shaw, and I. D. Aggarwal, *Opt. Lett.* **27**, 119 (2002).
²⁸R. W. Boyd, *Nonlinear Optics* (Academic, Amsterdam, 2008).
²⁹T. Cardinal, K. A. Richardson, H. Shim, A. Schulte, R. Beatty, K. Le Foulgoc, C. Meneghini, J. F. Viens, and A. Villeneuve, *J. Non-Cryst. Solids* **256-257**, 353 (1999).
³⁰F. Smektala, C. Quemard, V. Couderc, and A. Barthelemy, *J. Non-Cryst. Solids* **274**, 232 (2000).
³¹A. Prasad, C.-J. Zha, R.-P. Wang, A. Smith, S. Madden, and B. Luther-Davies, *Opt. Express* **16**, 2804 (2008).
³²A. Briley, M. R. Pederson, K. A. Jackson, D. C. Patton, and D. V. Porezag, *Phys. Rev. B* **58**, 1786 (1998).
³³H. Eckert, *Angew. Chem., Int. Ed. Engl.* **28**, 1723 (1989).
³⁴U. K. Vempati, M.S. thesis, University of Cincinnati, 2003.

- ³⁵D. G. Georgiev, P. Boolchand, H. Eckert, M. Micoulaut, and K. Jackson, *Europhys. Lett.* **62**, 49 (2003).
- ³⁶D. G. Georgiev, M. Mitkova, P. Boolchand, G. Brunklaus, H. Eckert, and M. Micoulaut, *Phys. Rev. B* **64**, 134204 (2001).
- ³⁷P. Boolchand, D. G. Georgiev, and M. Micoulaut, *J. Optoelectron. Adv. Mater.* **4**, 823 (2002).
- ³⁸R. Kerner and M. Micoulaut, *J. Non-Cryst. Solids* **210**, 298 (1997).
- ³⁹M. Micoulaut, in *Phase Transition and Self-organization in Electronic and Molecular Networks*, edited by J. C. Phillips and M. F. Thorpe (Kluwer Academic/Plenum, New York, 2001), p. 143.
- ⁴⁰M. Micoulaut, *C. R. Chim.* **5**, 825 (2002).
- ⁴¹L. Tichý and H. Tichá, *J. Non-Cryst. Solids* **189**, 141 (1995).
- ⁴²U. Vempati and P. Boolchand, *J. Phys.: Condens. Matter* **16**, S5121 (2004).
- ⁴³S. Chakravarty, D. G. Georgiev, P. Boolchand, and M. Micoulaut, *J. Phys.: Condens. Matter* **17**, L1 (2005).
- ⁴⁴J. P. Perdew and A. Zunger, *Phys. Rev. B* **23**, 5048 (1981).
- ⁴⁵M. R. Pederson and K. A. Jackson, *Phys. Rev. B* **41**, 7453 (1990).
- ⁴⁶K. Jackson and M. R. Pederson, *Phys. Rev. B* **42**, 3276 (1990).
- ⁴⁷G. B. Bachelet, D. R. Hamann, and M. Schlüter, *Phys. Rev. B* **26**, 4199 (1982).
- ⁴⁸D. Porezag and M. R. Pederson, *Phys. Rev. B* **54**, 7830 (1996).
- ⁴⁹T. B. Massalski and ASM International, *Binary Alloy Phase Diagrams* (ASM International, Materials Park, Ohio, 1990).
- ⁵⁰R. Blachnik, A. Hoppe, and U. Wickel, *Z. Anorg. Allg. Chem.* **463**, 78 (1980).
- ⁵¹R. Steudel and B. Eckert, in *Elemental Sulfur and Sulfur-Rich Compounds*, edited by R. Steudel (Springer-Verlag, Berlin, 2003), Vol. 1, p. 1.
- ⁵²R. Zallen, M. L. Slade, and A. T. Ward, *Phys. Rev. B* **3**, 4257 (1971).
- ⁵³K. Trentelman, L. Stodulski, and M. Pavlosky, *Anal. Chem.* **68**, 1755 (1996).
- ⁵⁴F. Marquez-Zavalía, J. R. Craig, and T. N. Solberg, *Can. Mineral.* **37**, 1255 (1999).
- ⁵⁵L. Bindi, V. Popova, and P. Bonazzi, *Can. Mineral.* **41**, 1463 (2003).
- ⁵⁶R. Steudel, in *Elemental Sulfur and Sulfur-Rich Compounds*, edited by R. Steudel (Springer-Verlag, Berlin, 2003), Vol. 1, p. 81.
- ⁵⁷P. Boolchand, M. Micoulaut, and P. Chen, in *Phase Change Materials: Science and Applications*, edited by S. Raoux and M. Wuttig (Springer, Heidelberg, 2008), p. 37.
- ⁵⁸P. Boolchand, P. Chen, D. I. Novita, and B. Goodman, in *Rigidity and Boolchand Intermediate Phases in Nanomaterials*, edited by M. Micoulaut and M. Popescu (INOE, Bucharest, Romania, 2009).
- ⁵⁹M. Frumar, Z. Polak, and Z. Cernosek, *J. Non-Cryst. Solids* **256-257**, 105 (1999).
- ⁶⁰D. Arsova, Y. C. Boulmetis, C. Raptis, V. Pamukchieva, and E. Skordeva, *Semiconductors* **39**, 960 (2005).
- ⁶¹M. Becucci, R. Bini, E. Castellucci, B. Eckert, and H. J. Jodl, *J. Phys. Chem. B* **101**, 2132 (1997).
- ⁶²T. Ohsaka and T. Ihara, *Phys. Rev. B* **50**, 9569 (1994).
- ⁶³R. Shuker and R. W. Gammon, *Phys. Rev. Lett.* **25**, 222 (1970).
- ⁶⁴S. N. Yannopoulos, K. S. Andrikopoulos, and G. Ruocco, *J. Non-Cryst. Solids* **352**, 4541 (2006).
- ⁶⁵G. Burns, *Solid State Physics* (Academic, Boston, 1990).
- ⁶⁶D. Selvanathan, W. J. Bresser, and P. Boolchand, *Phys. Rev. B* **61**, 15061 (2000).
- ⁶⁷T. Qu, D. G. Georgiev, P. Boolchand, and M. Micoulaut, in *Supercooled Liquids, Glass Transition and Bulk Metallic Glasses*, MRS Symposia Proceedings No. 754, edited by T. Egami, A. L. Greer, A. Inoue, and S. Ranganathan (Materials Research Society, Pittsburgh, 2003), p. 157.
- ⁶⁸K. Rompicharla, D. I. Novita, P. Chen, P. Boolchand, M. Micoulaut, and W. Huff, *J. Phys.: Condens. Matter* **20**, 202101 (2008).
- ⁶⁹M. Micoulaut and J. C. Phillips, *J. Non-Cryst. Solids* **353**, 1732 (2007).
- ⁷⁰M.-A. Brière, M. V. Chubynsky, and N. Mousseau, *Phys. Rev. E* **75**, 056108 (2007).
- ⁷¹M. F. Thorpe, D. J. Jacobs, M. V. Chubynsky, and J. C. Phillips, *J. Non-Cryst. Solids* **266-269**, 859 (2000).
- ⁷²D. N. Tafen and D. A. Drabold, *Phys. Rev. B* **71**, 054206 (2005).
- ⁷³P. Boolchand, X. Feng, and W. J. Bresser, *J. Non-Cryst. Solids* **293-295**, 348 (2001).
- ⁷⁴P. Boolchand, M. Jin, D. I. Novita, and S. Chakravarty, *J. Raman Spectrosc.* **38**, 660 (2007).
- ⁷⁵V. F. Kozhevnikov, J. M. Viner, and P. C. Taylor, *Phys. Rev. B* **64**, 214109 (2001).
- ⁷⁶P. Bonazzi, S. Menchetti, G. Pratesi, M. MunizMiranda, and G. Sbrana, *Am. Mineral.* **81**, 874 (1996).
- ⁷⁷E. Duval, A. Mermet, and L. Saviot, *Phys. Rev. B* **75**, 024201 (2007).
- ⁷⁸F. Leonforte, A. Tanguy, J. P. Wittmer, and J. L. Barrat, *Phys. Rev. Lett.* **97**, 055501 (2006).
- ⁷⁹S. N. Taraskin, Y. L. Loh, G. Natarajan, and S. R. Elliott, *Phys. Rev. Lett.* **86**, 1255 (2001).
- ⁸⁰K. S. Andrikopoulos, D. Christofilos, G. A. Kourouklis, and S. N. Yannopoulos, *J. Non-Cryst. Solids* **352**, 4594 (2006).
- ⁸¹A. Boukenter and E. Duval, *Philos. Mag. B* **77**, 557 (1998).
- ⁸²Y. C. Boulmetis, A. Perakis, C. Raptis, D. Arsova, E. Vateva, D. Nesheva, and E. Skordeva, *J. Non-Cryst. Solids* **347**, 187 (2004).
- ⁸³J. R. Smyth and T. C. McCormick, in *Mineral Physics and Crystallography: A Handbook of Physical Constants*, edited by T. J. Ahrens (AGU, Washington, D.C., 1995), p. 1.
- ⁸⁴A. L. Renninger and B. L. Averbach, *Acta Crystallogr., Sect. B: Struct. Crystallogr. Cryst. Chem.* **29**, 1583 (1973).